

Joint Spectrum Sensing and Direction of Arrival Recovery from sub-Nyquist Samples

Shahar Stein, Or Yair, Deborah Cohen, Yonina C. Eldar
Technion - Israel Institute of Technology, Haifa, Israel
{shaharst@t2, oryair@tx, debby@tx, yonina@ee}.technion.ac.il

Abstract—Joint spectrum sensing and direction of arrival (DOA) estimation is often necessary in communication applications, such as Cognitive Radio (CR). In this paper, we consider joint DOA and carrier frequency recovery of several transmissions as well as signal reconstruction from sub-Nyquist samples to overcome the sampling rate bottleneck of the wideband signals a CR typically deals with. We present two joint DOA and carrier frequency recovery approaches. The first is based on compressed sensing (CS) techniques and the second adapts a 2D-DOA recovery algorithm previously proposed in the Nyquist regime, the Parallel Factor (PARAFAC) analysis algorithm, to our sub-Nyquist samples. This technique allows us to solve the well known pairing issue between the DOA and carrier frequency to be recovered for each transmission. Once these are recovered, we show how the signal itself can be reconstructed from the samples. We also provide sufficient conditions for perfect blind signal recovery in terms of the sampling rate and the number of array elements.

I. INTRODUCTION

Spectrum sensing is a well-known task shared by many communication applications. Sometimes, the sole recovery of the signal support is not enough and both carrier frequency and direction of arrival (DOA) recovery are required. Cognitive Radio (CR) is such an example, whose aim is to solve the spectrum crowdedness [1], [2], [3]. Secondary users would opportunistically access frequency bands left vacant by their primary owners increasing spectral efficiency. Spectrum sensing is an essential task in the CR cycle [3]. Indeed, a CR should be able to constantly monitor the spectrum and detect the primary users (PUs) activity, reliably and fast [4], [5]. Moreover, DOA recovery would enhance the performance of CR by allowing it to exploit vacant bands, both spectrally and spatially.

Joint DOA and carrier frequency estimation has been considered in [6], [7], where the authors developed a joint angle-frequency estimation (JAFE) algorithm. JAFE is based on an extension of the ESPRIT algorithm [8] which allows for multiple parameters to be recovered. However, this method requires additional pairing between the carrier frequencies and the DOAs of the different transmissions. In [9], the authors consider multiple interleaved sampling channels, with a fixed delay between consecutive channels and propose a two-stage reconstruction, where the frequencies are first recovered and the DOAs are computed from their corresponding estimated carriers. Both works assume that the signal is sampled at least at its Nyquist rate and do not consider signal reconstruction.

To increase the chance of finding unoccupied spectral bands, CRs have to sense a wide spectrum band, leading to prohibitively high Nyquist rates which can even exceed today's best analog-to-digital converters (ADCs) bandwidths. Moreover, such high sampling rates generate a large number of samples to process, affecting speed and power consumption. A few works have recently considered joint

DOA and spectrum sensing from sub-Nyquist samples, assuming that the input signal is sparse in the frequency domain.

In [10], the authors exploit a mathematical relation between sub-Nyquist and Nyquist samples over a certain sensing time, whereas no specific sampling scheme is provided. The signal power spectrum is recovered from samples of an array, which is not necessarily a uniform linear array (ULA). Since the power spectrum is computed over a finite sensing time, the frequencies and angles are obtained on a grid defined by the number of samples. In [11], two interleaved L-shaped arrays, with a fixed delay between the two, sample the signal at a sub-Nyquist rate. Then, the carrier frequencies and the DOAs are recovered from the samples. However, the pairing issue between the two is not discussed. Moreover, this delay based approach suffers from the same drawbacks as the multicoset sampling scheme when it comes to practical implementation, as described in [12]. Specifically, the signal bandwidth can exceed the analog bandwidth of the ADC by orders of magnitude. Another practical issue stems from the time shift elements since it can be difficult to maintain accurate time delays between the ADCs at such high rates.

In this work, we consider several narrowband transmissions spread over a wide spectrum, impinging on an L-shaped ULA, each from a different direction. The array sensors are composed of an analog mixing front-end, implementing one channel of the modulated wideband converter (MWC) [12]. The signal is mixed by a periodic function, low-pass filtered and sampled at a low rate. We then propose two approaches to jointly recover the carrier frequencies and DOAs of the transmissions. The first is based on compressed sensing (CS) techniques that allow us to recover both parameters assuming they lie on a predefined grid. Particularly, we use the extended versions of orthogonal matching pursuit (OMP) and fast iterative shrinkage-thresholding algorithm (FISTA) adapted to sparse matrix recovery proposed in [13]. The second approach exploits the Parallel Factor (PARAFAC) analysis method [14], [15], previously proposed for the 2D-DOA problem. This approach solves the delicate issue of pairing between the two estimated angles. However, it has only been applied in the Nyquist regime so far. Here, we apply it on sub-Nyquist samples and extend it to the case where the second variable is a frequency rather than an additional angle. Once the carriers and DOAs are recovered, we show how the signal itself can be reconstructed. We also provide sufficient conditions on our sampling system for perfect reconstruction of the carriers and DOAs on the one hand, and of the signal itself on the other hand.

This paper is organized as follows. In Section II, we present the signal model and goal. Sections III and IV describe the sub-Nyquist sampling system and joint DOA estimation and spectrum sensing, respectively. Numerical experiments are presented in Section V.

II. SIGNAL MODEL AND GOAL

Consider a scenario with up to M complex-valued continuous-time transmissions $s_i(t)$, $i \in \{1, 2, \dots, M\}$, each modulated by

This work is supported in part by the Semiconductor Research Corporation (SRC) through the Texas Analog Center of Excellence (TxACE) at the University of Texas at Dallas (Task ID:1836.114), in part by the Israel Science Foundation under Grant no. 335/14, in part by the Ollendorf foundation, and in part by the Intel Collaborative Research Institute for Computational Intelligence (ICRI-CI). Deborah Cohen is grateful to the Azrieli Foundation for the award of an Azrieli Fellowship.

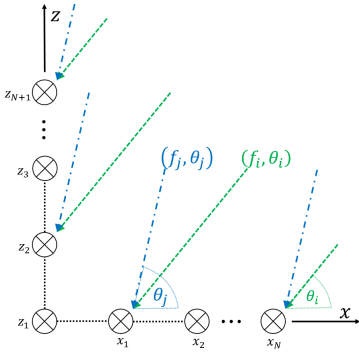


Fig. 1. An L-shaped array: N sensors along the x -axis and $N + 1$ sensors along the z -axis.

an unknown carrier frequency $f_i \in \mathbb{R}$. The source signals $s_i(t)$ are bandlimited to $\mathcal{B} = [-\frac{1}{2T}, \frac{1}{2T}]$ and disjoint, namely $\min_{i \neq j} \{|f_i - f_j|\} > B$, where $B = |\mathcal{B}| = \frac{1}{T}$. The modulated signals are bandlimited to $\mathcal{F} = [-\frac{f_{Nyq}}{2}, \frac{f_{Nyq}}{2}]$, that is $-\frac{f_{Nyq}+B}{2} \leq f_i \leq \frac{f_{Nyq}-B}{2}$.

The signals $s_i(t)$ are considered to be within the xz plane and are each associated to an unknown DOA, represented by an angle of arrival (AOA) θ_i , where θ_i is measured from the positive side of the x -axis and $|\theta_i| < 90^\circ$. All signals are assumed to be far-field, non coherent, and uncorrelated, i.e. $\mathbb{E}[s_i(t)\overline{s_j(t)}] = 0$ for $i \neq j$ and every t .

Each transmission $s_i(t)$ impinges on an L-shaped array with $2N + 1$ sensors in the xz plane, with its corresponding AOA θ_i , as shown in Fig. 1. The array consists of two orthogonal, uniform linear sub-arrays along the x and z -axis, with distance $d < \frac{f_{Nyq}}{c}$ between two adjacent sensors, where c is the speed of light.

Let $\mathbf{s}(t) = [s_1(t), s_2(t), \dots, s_M(t)]^T$ be the source signals vector, $\mathbf{S}(f) = [S_1(f), S_2(f), \dots, S_M(f)]^T$ be the signal Fourier transform vector, and $\mathbf{f} = [f_1, f_2, \dots, f_M]^T$, $\boldsymbol{\theta} = [\theta_1, \theta_2, \dots, \theta_M]^T$ be the carrier frequencies and AOAs vectors respectively. Our goal is to recover \mathbf{f} , $\boldsymbol{\theta}$ and the source signals $\mathbf{s}(t)$ from samples of the array output. We wish to design a sampling and reconstruction system which allows for perfect blind signal reconstruction, i.e. without any prior knowledge on the carrier frequencies nor the AOAs. In the next section, we describe the sampling scheme of our sensors.

III. SAMPLING SYSTEM

A. System Description

Our L-shaped array is composed of $2N + 1$ sensors which all have the same sampling pattern; the received signal is multiplied by a periodic function $p(t)$ with period $T_p = 1/f_p$, low-pass filtered with a filter that has cutoff-frequency f_s , and then sampled at the low rate f_s . In the next section, we show how we can recover \mathbf{f} , $\boldsymbol{\theta}$ and $\mathbf{s}(t)$ from these samples. We demonstrate that the minimal number of sensors required by our reconstruction method is $2N + 1 = 2M + 3$, with each sensor sampling at the minimal rate of $f_s = B$ to allow for perfect signal recovery. This leads to a minimal sampling rate of $(2M + 3)B$ which is assumed to be less than f_{Nyq} .

B. Frequency Domain Analysis

We now derive the relation between the sample sequences $x_n[k]$ and $z_n[k]$ from the x and z -axis respectively, and the unknown transmissions $s_i(t)$, carrier frequencies \mathbf{f} and AOAs $\boldsymbol{\theta}$. This analysis is used in the next section to derive our reconstruction schemes. We introduce the following definitions

$$\mathcal{F}_p \triangleq \left[-\frac{f_p}{2}, \frac{f_p}{2}\right], \quad \mathcal{F}_s \triangleq \left[-\frac{f_s}{2}, \frac{f_s}{2}\right].$$

Consider the received signal $u_n(t)$ at the n th sensor along the x -axis:

$$\begin{aligned} u_n(t) &= \sum_{i=1}^M s_i(t + \tau_n^x(\theta_i)) e^{j2\pi f_i(t + \tau_n^x(\theta_i))} \\ &\approx \sum_{i=1}^M s_i(t) e^{j2\pi f_i(t + \tau_n^x(\theta_i))}, \end{aligned} \quad (1)$$

where $\tau_n^x(\theta) = \frac{dn}{c} \cos(\theta)$ is the accumulated phase at the n th sensor with respect to the first sensor. The approximation in (1) stems from the narrow band assumption on the transmissions $s_i(t)$. The Fourier transform of the received signal $u_n(t)$ is then given by

$$U_n(f) = \sum_{i=1}^M S_i(f - f_i) e^{j2\pi f_i \tau_n^x(\theta_i)}. \quad (2)$$

In each sensor, the received signal is first mixed with the periodic function $p(t)$ prior to filtering and sampling. Since $p(t)$ is periodic with period $T_p = 1/f_p$, it can be represented by its Fourier series

$$p(t) = \sum_{l=-\infty}^{\infty} c_l e^{j2\pi l f_p t}, \quad (3)$$

where

$$c_l = \frac{1}{T_p} \int_0^{T_p} p(t) e^{-j2\pi l f_p t} dt. \quad (4)$$

The Fourier transform of the analog multiplication $\tilde{y}_n(t) = u_n(t)p(t)$ is evaluated as

$$\tilde{Y}_n(f) = \sum_{l=-\infty}^{\infty} c_l \cdot U_n(f - l f_p). \quad (5)$$

The mixed signal $\tilde{Y}_n(f)$ is a linear combination of f_p -shifted and c_l -scaled copies of $U_n(f)$. Substituting (2) in (5), we get

$$\tilde{Y}_n(f) = \sum_{l=-\infty}^{\infty} c_l \cdot \sum_{i=1}^M S_i(f - f_i - l f_p) e^{j2\pi f_i \tau_n^x(\theta_i)}.$$

Denote by $h(t)$ and $H(f)$ the impulse and frequency responses of an ideal LPF with cut-off frequency f_s , respectively. After filtering $\tilde{y}_n(t)$ with $h(t)$, we have

$$Y_n(f) = \begin{cases} \sum_{l=-\infty}^{\infty} c_l \sum_{i=1}^M S_i(f - f_i - l f_p) e^{j2\pi f_i \tau_n^x(\theta_i)}, & f \in \mathcal{F}_s \\ 0, & f \notin \mathcal{F}_s. \end{cases} \quad (6)$$

Since the source transmissions are bandlimited, namely $U_n(f) = 0$, $\forall f \notin \mathcal{F}$, the output $Y_n(f)$ involves only a finite number of aliases of $U_n(f)$. Consequently, we can write

$$Y_n(f) = \sum_{i=1}^M \tilde{S}_i(f) e^{j2\pi f_i \tau_n^x(\theta_i)}. \quad (7)$$

where L_0 is the smallest integer such that the sum contains all nonzero contributions, i.e. $L_0 = \left\lceil \frac{f_{Nyq} + f_s}{2f_p} \right\rceil - 1$, and

$$\tilde{S}_i(f) = \sum_{l=-L_0}^{L_0} c_l S_i(f - f_i - l f_p). \quad (8)$$

Note that in the interval \mathcal{F}_p , $\tilde{S}_i(f)$ is a cyclic shifted and scaled (by known factors $\{c_l\}$) version of $S_i(f)$, as shown in Fig. 2.

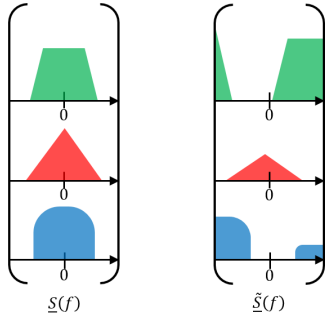


Fig. 2. The left pane shows the original source signals at baseband (before modulation). The right pane presents the output signals at baseband $\tilde{S}(f)$ after modulation, mixing and filtering.

After sampling, the discrete-time Fourier transform (DTFT) of the n th sequence $x_n[k] = y_n(kT_s)$ is expressed as

$$X_n(e^{j2\pi f T_s}) = \sum_{i=1}^M W_i(e^{j2\pi f T_s}) e^{j2\pi f_i \tau_n^x(\theta_i)}, \quad (9)$$

where we define $w_i[k] = \tilde{s}_i(kT_s)$ and $W_i(e^{j2\pi f T_s}) = \text{DTFT}\{w_i[k]\}$. It is convenient to write (9) in matrix form as

$$\begin{pmatrix} X_1(e^{j2\pi f T_s}) \\ X_2(e^{j2\pi f T_s}) \\ \vdots \\ X_N(e^{j2\pi f T_s}) \end{pmatrix} = \begin{pmatrix} e^{j2\pi f_1 \tau_1^x(\theta_1)} & \dots & e^{j2\pi f_M \tau_1^x(\theta_M)} \\ \vdots & & \vdots \\ e^{j2\pi f_1 \tau_N^x(\theta_1)} & \dots & e^{j2\pi f_M \tau_N^x(\theta_M)} \end{pmatrix} \begin{pmatrix} W_1(e^{j2\pi f T_s}) \\ W_2(e^{j2\pi f T_s}) \\ \vdots \\ W_M(e^{j2\pi f T_s}) \end{pmatrix},$$

or

$$\mathbf{X} = \mathbf{A}_x(\mathbf{f}, \theta) \cdot \mathbf{W}. \quad (10)$$

Similarly, when considering the received signal along the z -axis of the ULA, we get

$$\mathbf{Z} = \mathbf{A}_z(\mathbf{f}, \theta) \cdot \mathbf{W}, \quad (11)$$

where \mathbf{Z} is the sampled output signal in the frequency domain along the z -axis, and $\tau_n^z(\theta) = \frac{dn}{c} \sin \theta$, $n \in \{1, \dots, N+1\}$. Note that \mathbf{Z} is of length $N+1$, since the ULA along the z -axis has one additional sensor compared with the ULA along the x -axis. In the time domain, we have

$$\mathbf{x} = \mathbf{A}_x(\mathbf{f}, \theta) \cdot \mathbf{w} \quad (12)$$

$$\mathbf{z} = \mathbf{A}_z(\mathbf{f}, \theta) \cdot \mathbf{w}, \quad (13)$$

where \mathbf{x} and \mathbf{z} have n th element $x_n[k]$ and $z_n[k]$ respectively, and \mathbf{w} is a vector of length M with i th element $w_i[k]$.

In the following section we discuss possible methods to allow for unique recovery of \mathbf{f} and θ , present sufficient conditions to recover the transmissions $s(t)$ from \mathbf{w} , and provide a concrete reconstruction algorithm.

IV. JOINT DOA AND SPECTRUM RECONSTRUCTION

We begin by presenting two approaches for the recovery of the carrier frequencies and the AOAs. Then, once these are estimated, we show how we can reconstruct the transmissions $s_i(t)$ from the samples \mathbf{x} and \mathbf{z} .

A. Compressed Sensing Approach

Consider the correlation matrix \mathbf{R} between the samples along both axis, namely

$$\mathbf{R} = \mathbb{E}[\mathbf{z}\mathbf{z}^H] = \mathbf{A}_x \mathbf{R}_w \mathbf{A}_z^H, \quad (14)$$

where $\mathbf{R}_w = \mathbb{E}[\mathbf{w}\mathbf{w}^H]$ is a diagonal matrix with i th diagonal element $\mathbf{R}_{w_{ii}} = \mathbb{E}[|w_i|^2]$. This stems from the fact that the transmissions

are assumed to be uncorrelated. In the following, we assume perfect knowledge of \mathbf{R} . In practice, it can be estimated as

$$\mathbf{R} = \sum_{q=1}^Q \mathbf{x}_{(q)} \mathbf{z}_{(q)}^H, \quad (15)$$

where Q is the number of frames for the averaging, and $\mathbf{x}_{(q)}$ and $\mathbf{z}_{(q)}$ are the vectors of samples from both axis from the q th frame.

Denote $\alpha_i = f_i \cos \theta_i$ and $\beta_i = f_i \sin \theta_i$ and suppose that α_i and β_i lie on the grid $\{\delta l\}_{l=-L}^L$, with $L = \frac{f_{\text{Nyq}}}{2\delta}$. Here, δ is a parameter of the recovery algorithm that defines the grid resolution. We can then write

$$\mathbf{R} = \mathbf{B}\Phi\mathbf{C}^H, \quad (16)$$

where \mathbf{B} and \mathbf{C} are both $N \times (2L+1)$ matrices with (n, l) th element $B_{nl} = e^{j2\pi \frac{dn}{c} \alpha_l}$ and $C_{nl} = e^{j2\pi \frac{dn}{c} \beta_l}$, respectively, with $\alpha_l = \beta_l = \delta(l-L)$, $0 \leq l \leq 2L$. The nonzero elements of the $(2L+1) \times (2L+1)$ sparse matrix Φ are the M diagonal elements of \mathbf{R}_w at the M indices corresponding to $\{\alpha_i, \beta_i\}$. The goal is to recover the sparse matrix Φ from the $N \times (N+1)$ measurement matrix \mathbf{R} . To this end, we suggest to use CS algorithms for sparse matrix recovery.

1) *Joint carrier frequency and AOA recovery conditions*: The following theorem derives a necessary condition on the minimal number of sensors N for perfect recovery of $\alpha_i, \beta_i, i \in \{1, \dots, M\}$ in a noiseless environment.

Theorem 1. *If $d < \frac{f_{\text{Nyq}}}{c}$, the minimal number of sensors required for perfect recovery of Φ in (16) with M sources in a noiseless environment is $4M+3$.*

For lack of space, the proofs are omitted here. Theorem 1 is similar to Theorem 1 in [16] and can be proved by writing (16) in vector form and using the spark of Kronecker product from [17].

2) *Joint carrier frequency and AOA recovery*: To recover the sparse matrix Φ , we solve the following optimization problem [13]

$$\min \|\Phi\|_1 \text{ s.t. } \mathbf{B}\Phi\mathbf{C}^H = \mathbf{R}, \quad (17)$$

where $\|\Phi\|_1 = \sum_{i,j} |\Phi_{ij}|$ is the ℓ_1 -norm of $\text{vec}(\Phi)$. In [13], the authors consider a greedy based approach which extends the standard OMP to matrix form to solve (17).

With the noisy version of (16), we aim to solve the following ℓ_1 -norm minimization problem

$$\min_{\Phi} \left\{ \frac{1}{2} \|\mathbf{R} - \mathbf{B}\Phi\mathbf{C}^H\|_F^2 + \lambda \|\Phi\|_1 \right\}, \quad (18)$$

where λ is a regularization parameter and $\|\cdot\|_F$ denotes the Frobenius norm. The authors in [13] extend FISTA to sparse matrix recovery with matrix inputs. We can consider either the extended OMP or FISTA for sparse matrix recovery in order to solve (16). Once $\alpha_i, \beta_i, i \in \{1, \dots, M\}$ are recovered, the corresponding f_i and θ_i are given by

$$\begin{aligned} \hat{\theta}_i &= \tan^{-1} \left(\frac{\beta_i}{\alpha_i} \right), \\ \hat{f}_i &= \frac{\alpha_i}{\cos(\hat{\theta}_i)}. \end{aligned} \quad (19)$$

B. PARAFAC Analysis Approach

The joint DOA and carrier frequency recovery problem can also be treated as a 2D-DOA recovery problem, with the second variable being the frequency rather than an additional angle. The 2D-DOA problem requires both finding the two unknown angles, and pairing them. One effective solution relies on the trilinear model and PARAFAC analysis [14], [15].

1) *Preliminary Results:* A trilinear model as defined in [18] is a tensor \mathbf{T} with general element

$$t_{i,j,k} = \sum_{f=1}^F a_{i,f} b_{j,f} c_{k,f}. \quad (20)$$

Here, $a_{i,f}, b_{j,f}, c_{k,f}$ are elements of the matrices $\mathbf{A}, \mathbf{B}, \mathbf{C}$ accordingly, and F is called the loading factor. The matrices $\mathbf{A}, \mathbf{B}, \mathbf{C}$ can be recovered from the tensor \mathbf{T} using the PARAFAC analysis if the Kruskal condition [19] holds, namely

$$\kappa_{\mathbf{A}} + \kappa_{\mathbf{B}} + \kappa_{\mathbf{C}} \geq 2M + 2, \quad (21)$$

where $\kappa_{\mathbf{A}}$ denote the Kruskal rank of the matrix \mathbf{A} . In the next section, we show how we can formulate a trilinear model from (12)-(13) and how this model relates to the recovery of \mathbf{f} and θ .

2) *Trilinear Model:* Consider two sub-arrays along each axis; the first sub-array along the x -axis consists of the first $N - 1$ sensors, i.e. sensors $\{1, \dots, N - 1\}$ and the second one is composed of the last $N - 1$ sensors, i.e. $\{2, \dots, N\}$, along the same axis. Similarly, the first sub-array along the z -axis consists of sensors $\{1, \dots, N\}$, and the second one contains the last N sensors $\{2, \dots, N + 1\}$. For these sub-arrays, we have

$$\mathbf{x}_1 = \mathbf{A}_{x_1}(\mathbf{f}, \theta) \cdot \mathbf{w}, \quad \mathbf{x}_2 = \mathbf{A}_{x_2}(\mathbf{f}, \theta) \cdot \mathbf{w}, \quad (22)$$

$$\mathbf{z}_1 = \mathbf{A}_{z_1}(\mathbf{f}, \theta) \cdot \mathbf{w}, \quad \mathbf{z}_2 = \mathbf{A}_{z_2}(\mathbf{f}, \theta) \cdot \mathbf{w}. \quad (23)$$

Here, the vectors \mathbf{x}_1 and \mathbf{x}_2 contain the $N - 1$ first and last rows of \mathbf{x} and the matrices \mathbf{A}_{x_1} and \mathbf{A}_{x_2} are composed of the $N - 1$ first and last rows of \mathbf{A}_x , respectively. The corresponding vectors and matrices are similarly defined for the z -axis. From the properties of \mathbf{A}_x and \mathbf{A}_z , which are steering matrices of ULAs, it is easy to see that

$$\mathbf{A}_{x_2} = \mathbf{A}_{x_1} \Phi_1, \quad \mathbf{A}_{z_2} = \mathbf{A}_{z_1} \Phi_2, \quad (24)$$

where

$$\Phi_1 \triangleq \text{diag} \left(e^{j2\pi f_1 \tau_1^x(\theta_1)}, \dots, e^{j2\pi f_M \tau_1^x(\theta_M)} \right)$$

$$\Phi_2 \triangleq \text{diag} \left(e^{j2\pi f_1 \tau_1^z(\theta_1)}, \dots, e^{j2\pi f_M \tau_1^z(\theta_M)} \right).$$

Consider the following correlation matrices:

$$\mathbf{R}_1 \triangleq \mathbb{E} [\mathbf{x}_1 \mathbf{z}_1^H] = \mathbf{A}_{x_1} \mathbf{R}_w \mathbf{A}_{z_1}^H,$$

$$\mathbf{R}_2 \triangleq \mathbb{E} [\mathbf{x}_2 \mathbf{z}_1^H] = \mathbf{A}_{x_2} \mathbf{R}_w \mathbf{A}_{z_1}^H = \mathbf{A}_{x_1} \Phi_1 \mathbf{R}_w \mathbf{A}_{z_1}^H,$$

$$\mathbf{R}_3 \triangleq \mathbb{E} [\mathbf{x}_1 \mathbf{z}_2^H] = \mathbf{A}_{x_1} \mathbf{R}_w \mathbf{A}_{z_2}^H = \mathbf{A}_{x_1} \mathbf{R}_w \Phi_2^H \mathbf{A}_{z_1}^H,$$

$$\mathbf{R}_4 \triangleq \mathbb{E} [\mathbf{x}_2 \mathbf{z}_2^H] = \mathbf{A}_{x_2} \mathbf{R}_w \mathbf{A}_{z_2}^H = \mathbf{A}_{x_1} \Phi_1 \mathbf{R}_w \Phi_2^H \mathbf{A}_{z_1}^H.$$

Again, these matrices are assumed to be known but can be estimated as in (15). In order for the above correlation matrices to fit the trilinear model, we define the $4 \times M$ matrix \mathcal{R} whose k th column is given by

$$\mathcal{R}_k \triangleq \begin{bmatrix} R_{w_{kk}} \\ e^{j2\pi f_k \tau_1^x(\theta_k)} \cdot R_{w_{kk}} \\ e^{-j2\pi f_k \tau_1^z(\theta_k)} \cdot R_{w_{kk}} \\ e^{-j2\pi f_k \tau_1^x(\theta_k)} \cdot e^{j2\pi f_k \tau_1^z(\theta_k)} \cdot R_{w_{kk}} \end{bmatrix}. \quad (25)$$

Last, define the 3D tensor, $\Delta_{N \times (N-1) \times 4}$, with its k th slice $\Delta_k = \mathbf{R}_k$, $k \in \{1, \dots, 4\}$ as follows

$$\Delta_k = \mathbf{R}_k = \mathbf{A}_{x_1} \text{diag} \left[(\mathcal{R}^T)_k \right] \mathbf{A}_{z_1}^H. \quad (26)$$

It can then be easily seen that the typical element of Δ is given by

$$\Delta_{i,j,k} = \sum_{m=1}^M a_{i,m} b_{j,m} c_{k,m}, \quad (27)$$

where $a_{i,m}$ denotes the (i, m) th element of \mathbf{A}_{x_1} , $b_{j,m}$ denotes the (j, m) th element of \mathbf{A}_{z_1} and $c_{k,m}$ denotes the (k, m) th element of \mathcal{R} . Therefore, the tensor Δ follows the trilinear model, with its trilinear decomposition given by (27).

3) *Reconstruction Conditions:* The following theorem presents sufficient conditions for the perfect recovery of \mathcal{R} from Δ .

Theorem 2. *If:*

- $f_i \cos \theta_i \neq f_j \cos \theta_j + k$, $\forall k$, for every $i \neq j$,
- $f_i \sin \theta_i \neq f_j \sin \theta_j + k$, $\forall k$, for every $i \neq j$,
- $d < \frac{c}{f_{\text{Nyq}}}$,
- $N \geq M + 1$,

then, $(\hat{\mathbf{f}}, \hat{\theta})$ can be uniquely recovered from Δ , as defined in (27).

The proof of Theorem 2 relies on showing that the Kruskal condition holds here. The steering matrices are Vandermonde and therefore full Kruskal rank and it can be easily shown that under the above conditions, the Kruskal rank of \mathcal{R} is at least 2. Therefore, \mathcal{R} , and as a consequence $(\hat{\mathbf{f}}, \hat{\theta})$, can be uniquely recovered from Δ , as shown below.

4) *Reconstruction Method:* One possible method for solving the trilinear model is the PARAFAC [18] algorithm, whose concept we now briefly describe. Consider the following matrices: $\mathbf{A}_{I \times F}, \mathbf{B}_{J \times F}, \mathbf{C}_{K \times F}$ and the tensor $\mathbf{D}_{I \times J \times K}$ such that $D_{i,k,j} = \sum_{f=1}^F a_{i,f} b_{j,f} c_{k,f}$. The goal is to decompose \mathbf{D} to $\mathbf{A}, \mathbf{B}, \mathbf{C}$. The trilinear model (20) can be written as a bilinear model by unfolding the tensor \mathbf{D} along some dimension, e.g. $\mathbf{D}_{I \times J \times K} = \mathbf{A} \cdot \mathbf{Z}$, where $\mathbf{Z}_{F \times J \times K}$ is a matrix with its l th row defines by $\mathbf{z}_l^T \triangleq [\mathbf{b}_l \otimes \mathbf{c}_l]^T$, where \otimes is the Kronecker product operation. The algorithm iteratively estimates each of the matrices $\mathbf{A}, \mathbf{B}, \mathbf{C}$ using the Alternative Least Square (ALS) method. Convergence is determined by a threshold or maximum iterations number. Once \mathcal{R} is recovered from Δ , $(\hat{\mathbf{f}}, \hat{\theta})$ is given by (19), where α_i and β_i are defined as

$$\alpha_i = f_i \cos(\theta_i) = \frac{c}{2\pi d} \cdot \angle \frac{\mathcal{R}_{2,i}}{\mathcal{R}_{1,i}} \quad (28)$$

$$\beta_i = f_i \sin(\theta_i) = \frac{c}{2\pi d} \cdot \angle \frac{\mathcal{R}_{3,i}}{\mathcal{R}_{1,i}}. \quad (29)$$

C. Perfect Blind Spectrum Reconstruction

Once $(\hat{\mathbf{f}}, \hat{\theta})$ are recovered, we can construct either of the steering matrices which are both full column rank from the Kruskal rank condition (21), and $\hat{\mathbf{w}}$ is obtained as follows

$$\hat{\mathbf{w}} = \mathbf{A}_x^\dagger(\hat{\mathbf{f}}, \hat{\theta}) \mathbf{x}. \quad (30)$$

The following theorem presents the conditions for \mathbf{s} to be uniquely reconstructed from \mathbf{w} .

Theorem 3. *Let $(\hat{\mathbf{f}}, \hat{\theta}, \hat{\mathbf{w}})$ be the unique solution of (12) and (13). If:*

- $c_l \neq 0 \quad \forall l \in \{-L_0, \dots, L_0\}$, where c_l is defined in (4),
- $f_s = f_p \geq B$

then, $\{\hat{s}_i\}_{i=1}^M$ can be uniquely recovered from \mathbf{w} .

Theorem 3 guarantees that no information is lost in the analog preprocessing, namely there an is injective mapping from \mathbf{w} to \mathbf{s} , and s_i can be uniquely recovered from w_i as

$$\hat{S}_i(f) = \frac{1}{c_{l_a}} W_i \left(e^{j2\pi(f+f_i+l_a \cdot f_p)T_s} \right), \quad f \in \mathcal{B}, \quad (31)$$

where $l_a = \left\lfloor \frac{f_i}{f_p} \right\rfloor + f$.

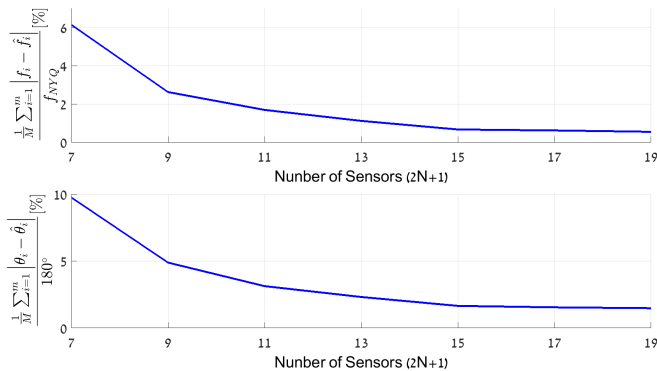


Fig. 3. Carrier frequency and AOA reconstruction performance vs. total number of sensors $2N + 1$, with $SNR = 10\text{dB}$, $Q = 300$, $M = 3$.

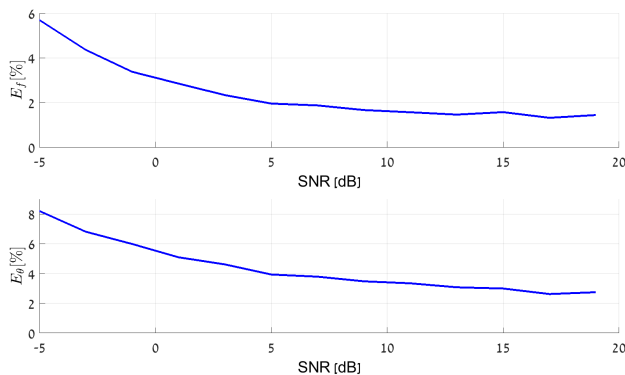


Fig. 4. Carrier frequency and AOA reconstruction performance vs. SNR, with $2N + 1 = 11$, $Q = 300$, $M = 3$.

V. SIMULATIONS

In this section, we demonstrate the reconstruction of the PARAFAC analysis approach only, for lack of space. Consider $M = 3$ complex-valued narrowband source signals $s_i(t)$, $i = 1, 2, 3$, each of width $B = 50\text{MHz}$ and with $f_{\text{Nyq}} = 10\text{GHz}$. The carrier frequencies f_i and AOAs θ_i are drawn uniformly at random from $[-\frac{f_{\text{Nyq}}-B}{2}, \frac{f_{\text{Nyq}}-B}{2}]$, and $[-85^\circ, 85^\circ]$, respectively. The L-shaped array is composed of $2N + 1$ sensors; N along the x -axis, and $N + 1$, along the z -axis, with mixing and sampling rates $f_s = f_p = 1.2B$. We use mixing function $p(t) = \sum_{l=-\infty}^{\infty} \delta(t - \frac{l}{f_p})$. Note that in the case where $M = 3$, the minimal required number of sensors is $2M + 3 = 9$. The received signal at each sensor is corrupted with additive white Gaussian noise (AWGN). To recover the carrier frequencies and AOAs from the the input samples, we use the COMFAC MATLAB function implemented in [20].

The first simulations focus on the recovery of the carrier frequencies f_i and AOAs θ_i . The reconstruction performance is measured by the following criteria: $E_f = \frac{1}{M} \sum_{i=1}^M |f_i - \hat{f}_i|$ for the frequencies, and $E_\theta = \frac{1}{M} \sum_{i=1}^M |\theta_i - \hat{\theta}_i|$ for the AOAs.

The first simulation examines the recovery performance with respect to the number of sensors $2N + 1$. Figure 3 presents the carrier frequency and AOA reconstruction performance for different values of the latter. The second simulation, presented in Fig. 4, illustrates the impact of SNR on the recovery performance. Last, Fig. 5 demonstrates signal reconstruction and shows the normalized mean square error (MSE) of the estimator with respect to its maximal value $\frac{\mathbb{E} \|s - \hat{s}\|^2}{\max \mathbb{E} \|s - \hat{s}\|^2}$ under different SNR scenarios.



Fig. 5. Signal reconstruction performance vs. SNR, with $2N + 1 = 25$, $Q = 500$, $M = 3$.

REFERENCES

- [1] J. Mitola, "Software radios: Survey, critical evaluation and future directions," *IEEE Aerosp. Electron. Syst. Mag.*, vol. 8, pp. 25–36, Apr. 1993.
- [2] S. Haykin, "Cognitive radio: Brain-empowered wireless communications," *IEEE J. Select. Areas Commun.*, vol. 23, pp. 201–220, Feb. 2005.
- [3] A. Ghasemi and E. S. Sousa, "Spectrum sensing in cognitive radio networks: requirements, challenges and design trade-offs," *IEEE Communications Magazine*, vol. 46, pp. 32–39, Apr. 2008.
- [4] E. G. Larsson and M. Skoglund, "Cognitive radio in a frequency-planned environment: Some basic limits," *IEEE Trans. Wireless Commun.*, vol. 7, pp. 4800–4806, Dec. 2008.
- [5] N. H. A. Sahai and R. Tandra, "Some fundamental limits on cognitive radio," *Proc. 42nd Annu. Allerton Conf. Commun., Control, and Computing*, pp. 1662–1671, Oct. 2004.
- [6] A. N. Lemma, A. van der Veen, and E. F. Deprettere, "Joint angle-frequency estimation using multi-resolution ESPRIT estimation," *IEEE ICASSP*, pp. 1957–1960, May 1998.
- [7] —, "Analysis of joint angle-frequency estimation using ESPRIT," *IEEE Journal of Selected Topics in Signal Processing*, vol. 51, pp. 1264–1283, May 2003.
- [8] A. Paulraj, R. Roy, and T. Kailath, "Estimation of signal parameters via rotational invariance techniques - ESPRIT," *Information Systems Laboratory*, 1986.
- [9] W. Xudong, X. Zhang, J. Li, and J. Bai, "Improved ESPRIT method for joint direction-of-arrival and frequency estimation using multiple-delay output," *International Journal of Antennas and Propagation*, Jul. 2012.
- [10] D. D. Ariananda and G. Leus, "Compressive joint angular-frequency power spectrum estimation," *IEEE EUSIPCO*, pp. 1–5, Sep. 2013.
- [11] A. A. Kumar, S. G. Razul, and C. S. See, "An efficient sub-Nyquist receiver architecture for spectrum blind reconstruction and direction of arrival estimation," *IEEE ICASSP*, pp. 6781–6785, May 2014.
- [12] M. Mishali and Y. C. Eldar, "From theory to practice: Sub-Nyquist sampling of sparse wideband analog signals," *IEEE Journal of Selected Topics in Signal Processing*, vol. 4, no. 2, pp. 375–391, Apr. 2010.
- [13] T. Wimalajeewa, Y. C. Eldar, and P. K. Varshney, "Recovery of sparse matrices via matrix sketching," *CoRR*, vol. abs/1311.2448, 2013. [Online]. Available: <http://arxiv.org/abs/1311.2448>
- [14] X. Zhang, J. Li, and L. Xu, "Novel two-dimensional doa estimation with l-shaped array," *EURASIP Journal on Advances in Signal Processing*, vol. 2011, no. 50, Aug. 2011.
- [15] D. Liu and J. Liang, "L-shaped array-based 2-d doa estimation using parallel factor analysis," *World Congress on Intelligent Control and Automation (WCICA)*, pp. 6949–6952, Jul. 2010.
- [16] D. Cohen, A. Dikopoltsev, and Y. C. Eldar, "Extensions of sub-nyquist radar: Reduced time-on-target and cognitive radar," *International Workshop on Compressed Sensing Theory and its Applications to Radar, Sonar and Remote Sensing (CoSeRa)*, Jun. 2015.
- [17] S. Jokar and V. Mehrmann, "Sparse solutions to underdetermined Kronecker product systems," *Linear Algebra and its Applications*, vol. 431, no. 12, pp. 2437 – 2447, 2009.
- [18] R. A. Harshman and M. E. Lundy, "Parafac: Parallel factor analysis," *Computational Statistics & Data Analysis*, vol. 18, no. 1, pp. 39–72, 1994.
- [19] A. Stegeman and N. Sidiropoulos, "On kruskal uniqueness condition for the candecomp/parafac decomposition," *Linear Algebra and its Applications*, vol. 420, no. 2-3, pp. 553–571, Jan. 2007.
- [20] N. D. Sidiropoulos, "Comfac: Matlab code for ls fitting of the complex parafac model in 3-d," <http://www.telecom.tuc.gr/~nikos>, 1998.